

## Catalytic Aerobic Oxidation of Alkenes by Ag@Metal Organic Framework with High Catalytic Activity and Selectivity

H. Salari\*

*Department of Chemistry, College of Sciences, Shiraz University, Shiraz, Iran*

*(Received 21 June 2019, Accepted 22 August 2019)*

By coupling of  $\text{Fe}_2\text{O}_3@\text{SiO}_2$  particles with metal organic framework (MOF) the magnetic MOF structure was fabricated. Precipitation and hydrothermal methods were applied for the synthesis of core and MOF. Silver nanoparticles were deposited on nickel based metal organic framework surface and magnetic  $\text{Fe}_2\text{O}_3@\text{SiO}_2@\text{MOF}@Ag$  was obtained. Because of strong coupling between silver nanoparticles and metal organic framework, the catalyst demonstrated high catalytic activity and selectivity in aerobic oxidation of alkenes under mild conditions. The nanostructure, exhibited high catalytic activity. Alkenes oxides (epoxy alkanes) were the main products with more than 89.9% selectivity.

**Keywords:** Metal organic frame-work, Aerobic oxidation, Magnetic structure

### INTRODUCTION

In metal organic frameworks (MOFs), organic linkers and transition metals create building blocks with two or three dimensional networks. These porous class of materials offer active sites with reasonable properties like well-defined pore structure, high micropore volume, high resistant to structure collapse and flexibility in structure design. Low thermal stability of organic linkers limits their applications in high temperature gas phase reactions. Catalytic reactions in liquid phase under 600 K [1] could be examined very well. In recent years, MOFs have been widely used in catalysis [2-4], electrochemistry [5,6], solar cells [7,8], electronics and photonics [9,10] and hydrogen storage [11,12]. MOFs are considered as host matrices for nanoparticles synthesis, and as templates for material fabrication [13]. Because of high porosity of MOF, metal nanoparticles could be embedded. Metal@MOF system subsequently could be used in heterogeneous processes such as condensation, hydrogenations, carbon-carbon coupling, aerobic oxidation and chemical  $\text{H}_2$  storage [14,15]. Exterior

and interior control of solid state materials have been big habitual challenge in material chemistry field. One of the most important challenges for chemist in material science is controlling the interior of structure and then transforming them into the sophisticated forms like truncated cube because this new faced material could demonstrate advanced functional properties in catalysis. This study is based on a new magnetic core shell structure referred as porous coordination polymers or metal organic frameworks. Silver nanoparticles synthesize with strong catalytic activity and monodispersity is difficult compare to other nanoparticles, because Ag has more tendency for aggregation and control of size and shape is now a big challenge. Reduction temperature, loading time, concentration of metal precursor, reduction agent, washing, drying and calcination conditions are some major parameters affect the size of Ag nanoparticles. There are several methods to embed metals in MOF structures. Impregnation with chloride and nitrate salt of metals which followed by reduction is most popular method [16,17]. Chemical vapor deposition (followed by hydrogenolysis and thermal decomposition) [18,19], UV [20], visible [21] and microwave [22] irradiations to metal ions, grinding solid

\*Corresponding author. E-mail: [hsalari@shirazu.ac.ir](mailto:hsalari@shirazu.ac.ir)

precursor with MOF [23], and encapsulation of presynthesized metal in MOF [24] are some of other technics for preparation of metal@MOF.

Epoxidation reactions with production of prevalent compounds like  $\alpha$ -hydroxyketones and 1,2-dicarbonyl alkyl play important role in material industries. Using molecular oxygen in oxidation reaction would be important because of environmentally friendly nature of  $O_2$  and purification of products. Improving the epoxidation reaction catalysts operating at mild conditions in liquid phase with molecular oxygen is desirable. Although many reports issued for oxidation of hydrocarbons and alkenes, oxygenation of alkenes with dioxygen stay unexplored. In this work, for the first time the aerobic oxidation of alkenes by novel magnetic core MOF@Ag was investigated and the catalysts demonstrated high activity and selectivity.

## EXPERIMENTAL

### Materials

$AgNO_3$ ,  $FeCl_3 \cdot 6H_2O$ , NaOH,  $NaBH_4$ ,  $NH_3$ , Dimethyl formamide (DMF), Tetraethylorthosilicate (TEOS) were from Sigma-Aldrich (st. Louis, Mo) and  $Ni(NO_3)_2 \cdot 6H_2O$ , and benzene-1,3,5-tricarboxylic acid (Trimesic acid ( $H_3BTC$ )) were obtained from Merck without any purification.

### Preparation of Catalysts

$Fe_2O_3$  nanoparticles were fabricated by chemical reduction method.  $FeCl_3 \cdot 6H_2O$  was dissolved in DI water and by adjusting the pH at 7, NaOH solution was added dropwise. The mixture was stirred vigorously for 6 h at room temperature. Then, aqueous solution of  $NaBH_4$  slowly was added and the mixture stirred for 4 h. The synthesized  $Fe_2O_3$  was washed several times with water and ethanol respectively and the brown product was dried in oven for 12 at 85 °C.

For fabrication of  $Fe_2O_3@SiO_2$ , 0.6 g of  $Fe_2O_3$  powder was dispersed in 20 ml of water and sonicated for 30 min. 15 ml of  $NH_3$  (25%) and 25 ml of ethanol were added to brown suspension. Then, 5 ml of TEOS slowly, drop by drop, was added to mixture and stirred for 8 h vigorously at room temperature. The light gray powder washed three times with water and ethanol and dried at 90 °C for 10 h.

For preparation of  $Fe_2O_3@SiO_2@MOF$ , 0.4 g benzene-

1,3,5-tricarboxylic acid was dissolved in N,N-dimethylformamide. In another vessel, 0.5 g  $Ni(NO_3)_2 \cdot 6H_2O$  was dissolved in N,N-dimethylformamide (DMF). Two solutions were mixed together and the final solution was stirred for 5 h at 45 °C. Then, 0.15 g  $Fe_2O_3@SiO_2$  was added to mixture. The suspension was sonicated for 30 min and after 1 h stirring, the mixture poured to teflon lined autoclave. The autoclave was kept at 160 °C for 24 h. The prepared catalyst was separated by filtration and washed several times with ethanol and water, respectively.  $Fe_2O_3@SiO_2@MOF$  structure dried in an oven at 80 °C for 12 h.

For preparation of  $Fe_2O_3@SiO_2@MOF@Ag$ ,  $Fe_2O_3@SiO_2@MOF$  should be desolvated to ensure the DMF removal.  $Fe_2O_3@SiO_2@MOF$  kept at 110 °C for 2 h under vacuum. The desolvated green powder was immersed in 40 ml methanolic solution of  $AgNO_3$  and stirred at 70 °C to all solvent evaporated. Ethanolic solution of  $NaBH_4$  was applied to reduce the  $Ag^+$  ion and produce  $Fe_2O_3@SiO_2@MOF@Ag$ . The final product was separated and dried in 80 °C over a night. Different weight percentages of silver on  $Fe_2O_3@SiO_2@MOF$  structure were synthesized by similar procedure and using various amounts of silver.

### Catalytic Reaction

A stirred batch reactor with 5 cm<sup>3</sup> capacity was applied for oxidation of alkenes under 5 bar pressure of oxygen gas. Toluene was used as solvent (3 ml) and the reaction was carried out by contacting the catalysts with 0.1 ml of alkenes under vigorous stirring at 85 °C for 6 h. GC-FID equipped with HP5 column was used for analyzing the products and unconverted reactant. Helium was the carrier gas.

### Characterization of Catalysts

Crystallinity and phase structure of  $Fe_2O_3$ ,  $Fe_2O_3@SiO_2$  and  $Fe_2O_3@SiO_2@MOF@Ag$  powders were analyzed by X-ray diffraction (XRD) method. The XRD patterns were recorded by Bruker D<sub>8</sub> with Cu K<sub>α</sub> irradiation. Catalyst morphology was investigated by scanning electron microscope (SEM) (KYKY-EM3200). Material specific surface area was determined using the Brunauer-Emmett-Teller (BET) method based on  $N_2$  adsorption-desorption at 77 K using Belsorp apparatus. The photocatalysts first were

dried at 80 °C and degased at 180 °C for 2 h. The BET plots in the pressure range of 0.05-1 were achieved and  $P/P_0 = 0.99$  was picked out for measuring the pore volume. The surface composition and chemical state of elements were monitored by X-ray photoelectron spectroscopic (XPS) analysis (Bestec). The size of nanostructure particles was measured by transmission electron microscopy (TEM) model CM120 Philips. Differential thermal analysis (DTA) and thermogravimetric analysis (TGA) by SDT Q600 instruments were used for  $\text{Fe}_2\text{O}_3@\text{SiO}_2@\text{MOF}@Ag$  characterization.

## RESULTS AND DISCUSSION

TGA curve and corresponding DTA curve can be divided into three stages. As can be seen in Fig. 1, the first stage is related to moisture evaporation and gas desorption. The second stage reflects the DMF removal from MOF structure and third stage is attributed to MOF pyrolysis. It can be concluded from TGA-DTA curve of  $\text{Fe}_2\text{O}_3@\text{SiO}_2@\text{MOF}@Ag$  that MOF is stable thermally until 360°C. After removal of organic part of MOF, no any changes were observed for this structure. The XRD patterns of  $\text{Fe}_2\text{O}_3$ ,  $\text{Fe}_2\text{O}_3@\text{SiO}_2$ ,  $\text{Fe}_2\text{O}_3@\text{SiO}_2@\text{MOF}$  and  $\text{Fe}_2\text{O}_3@\text{SiO}_2@\text{MOF}@Ag$  are shown in Fig. 1. Sharp diffraction peaks at  $2\theta = 24, 33, 35, 42, 50, 54, 57, 63, 64$  and  $72$  are assigned to 012, 104, 110, 113, 024, 116, 122, 213, 300 and 101 planes of  $\text{Fe}_2\text{O}_3$  structure with reference number of JCPDS NO. 01-1030. Another observation that can be found in Figure 2 is that the  $\text{Fe}_2\text{O}_3@\text{SiO}_2$  composite has similar XRD pattern as  $\alpha\text{-Fe}_2\text{O}_3$ . This similar pattern indicates that crystal structure of  $\text{Fe}_2\text{O}_3$  after silica coating has not been changed. The peaks at the diffraction angle  $2\theta$ : 38, 44 and 65 are corresponded to (111), (200) and (200) set of lattice planes of Ag (JCPDS files no. 04-0783). There are several factors affecting the crystallinity and morphology of Ni-BTC metal organic frameworks. The solvents, precursor type, reaction modes, pH, temperature and concentration are the main factors able to change the MOF structure. In different solvents, Ni-based MOF has different crystal structures [25,26]. The nitrogen adsorption-desorption isotherms of  $\text{Fe}_2\text{O}_3$ ,  $\text{Fe}_2\text{O}_3@\text{SiO}_2$ ,  $\text{Fe}_2\text{O}_3@\text{SiO}_2@\text{MOF}$  and  $\text{Fe}_2\text{O}_3@\text{SiO}_2@\text{MOF}@Ag$  are shown in Fig. 2 and the results are reported in Table 1.

All isotherms are type II according to the BET classification with contribution of mesopores and hysteresis loop which is a signature for mesoporous structures appeared in adsorption-desorption measurements [27,28]. Introduction of  $\text{Fe}_2\text{O}_3$  with  $\text{SiO}_2$  led to higher surface area. High porosity of formed  $\text{SiO}_2$  caused high specific surface area creation for fabrication of porous MOF. Surface area of  $79.9 \text{ m}^2 \text{ g}^{-1}$  and pore volume of  $0.16 \text{ cm}^3 \text{ g}^{-1}$  was achieved for  $\text{Fe}_2\text{O}_3@\text{SiO}_2@\text{MOF}@Ag$ .

$\text{Fe}_2\text{O}_3$  and  $\text{Fe}_2\text{O}_3@\text{SiO}_2$  demonstrate wide pore size distribution in the range of 25-50 nm. The wide distribution of pore size is originated from chemical interactions between  $\text{Fe}_2\text{O}_3$  and  $\text{Fe}_2\text{O}_3@\text{SiO}_2$ . The pore volumes were  $1.02$  and  $0.42 \text{ cm}^3 \text{ g}^{-1}$  for  $\text{Fe}_2\text{O}_3$  and  $\text{Fe}_2\text{O}_3@\text{SiO}_2$ , respectively. Narrow size distributions ( $\sim 2$  nm) was observed for  $\text{Fe}_2\text{O}_3@\text{SiO}_2@\text{MOF}$  and  $\text{Fe}_2\text{O}_3@\text{SiO}_2@\text{MOF}@Ag$ . Pore volume for  $\text{Fe}_2\text{O}_3@\text{SiO}_2@\text{MOF}$  and  $\text{Fe}_2\text{O}_3@\text{SiO}_2@\text{MOF}@Ag$  are  $0.16 \text{ cm}^3 \text{ g}^{-1}$ .

The morphology of  $\text{Fe}_2\text{O}_3@\text{SiO}_2@\text{MOF}@Ag$  was investigated and shown across the scanning electron microscopy (SEM) images in Fig. 3 and as can be seen the 3D dendritic fibrous nano

MOF is synthesizes successfully. This is confirmed by TEM analysis that average diameter of Ag NPs was 25 nm and the shape of the NPs is largely spherical.

The chemical composition and electronic structure of the porous  $\text{Fe}_2\text{O}_3@\text{SiO}_2@\text{MOF}@Ag$  was investigated by X-ray photoelectron spectroscopy. Smoothing and background subtraction of raw peaks were performed by the Gaussian software, and analyzing and deconvolution were done by the Origin Ver. 8.1 software. The presence of nickel, oxygen, carbon and silver was approved by X-ray photoelectron spectroscopy. Two main peaks located at 368 and 374 are related to  $\text{Ag}3d_{5/2}$  and  $\text{Ag}3d_{3/2}$  of silver in  $\text{Ag}^0$  state (Fig. 3, C, D).

The magnetic properties of the samples were measured by vibration sample magnetometer (VSM) technique. The magnetization curve of samples are illustrated in Fig. 4. Super-paramagnetic behavior with hysteresis loop was observed. The saturation magnetization values of 40 and 30  $\text{emu g}^{-1}$  for  $\text{Fe}_2\text{O}_3$  and  $\text{Fe}_2\text{O}_3@\text{SiO}_2@\text{MOF}@Ag$  were observed, respectively. Introduction of iron oxide core with  $\text{SiO}_2@\text{MOF}$  structure reduced the maximum saturation

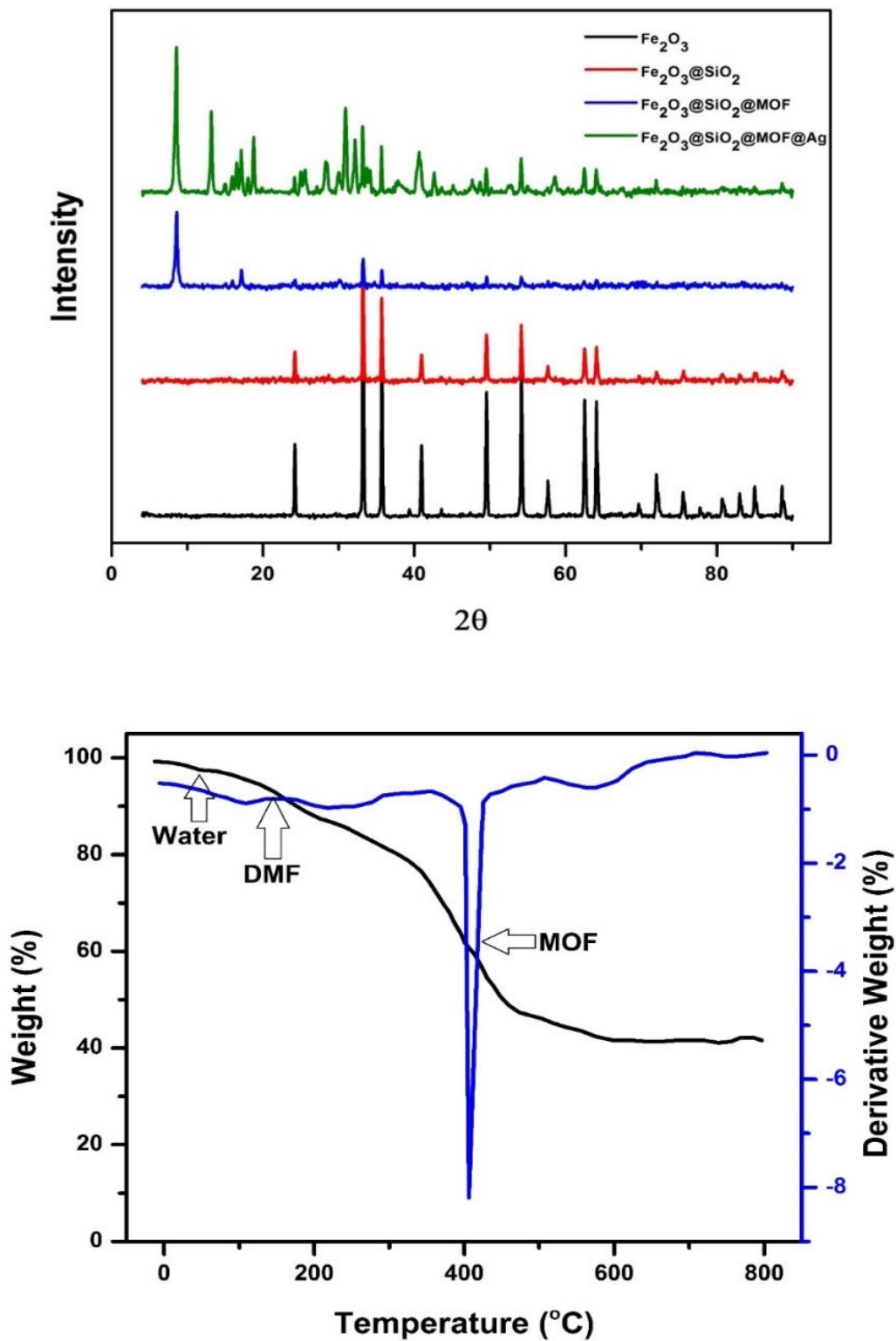
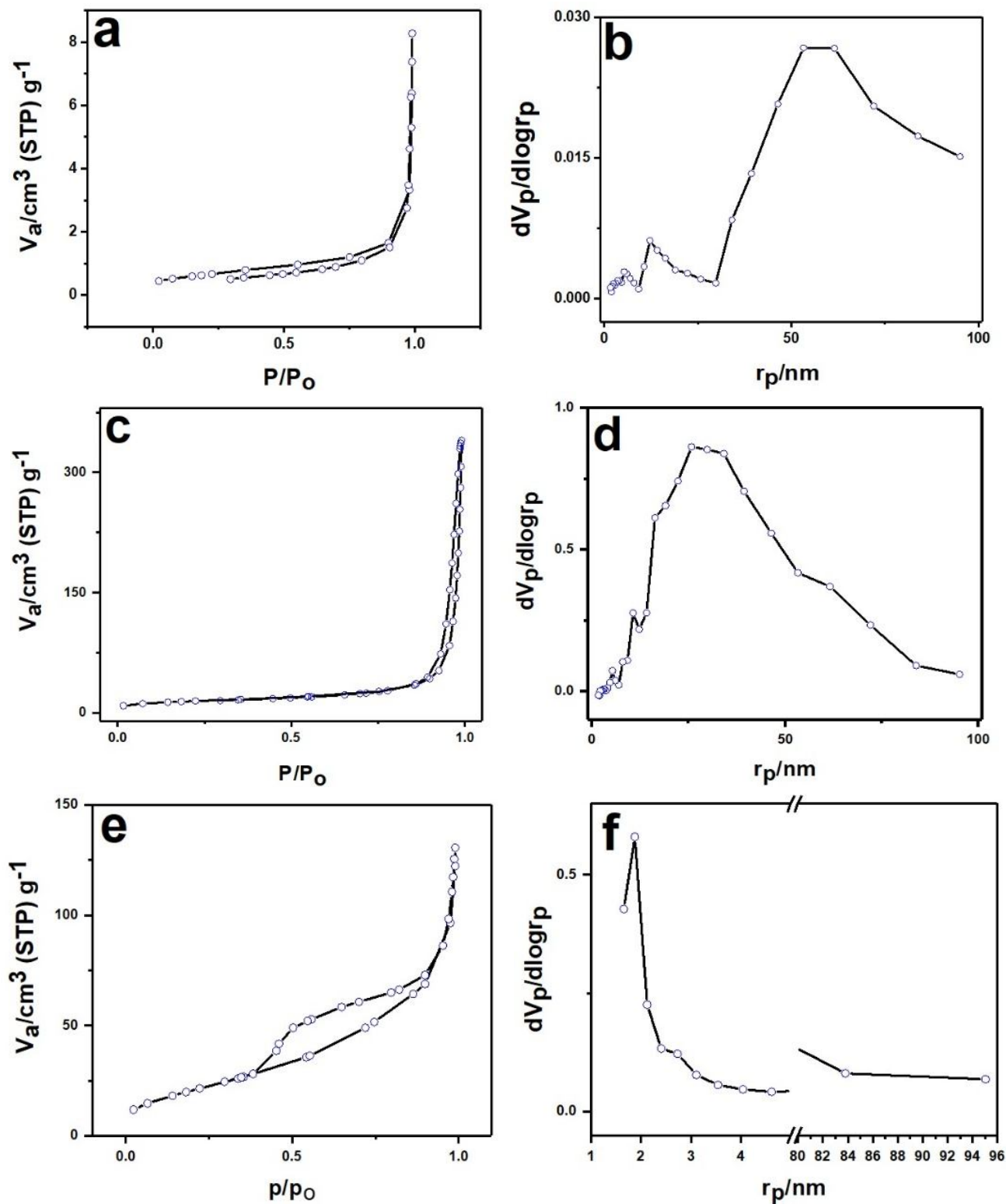


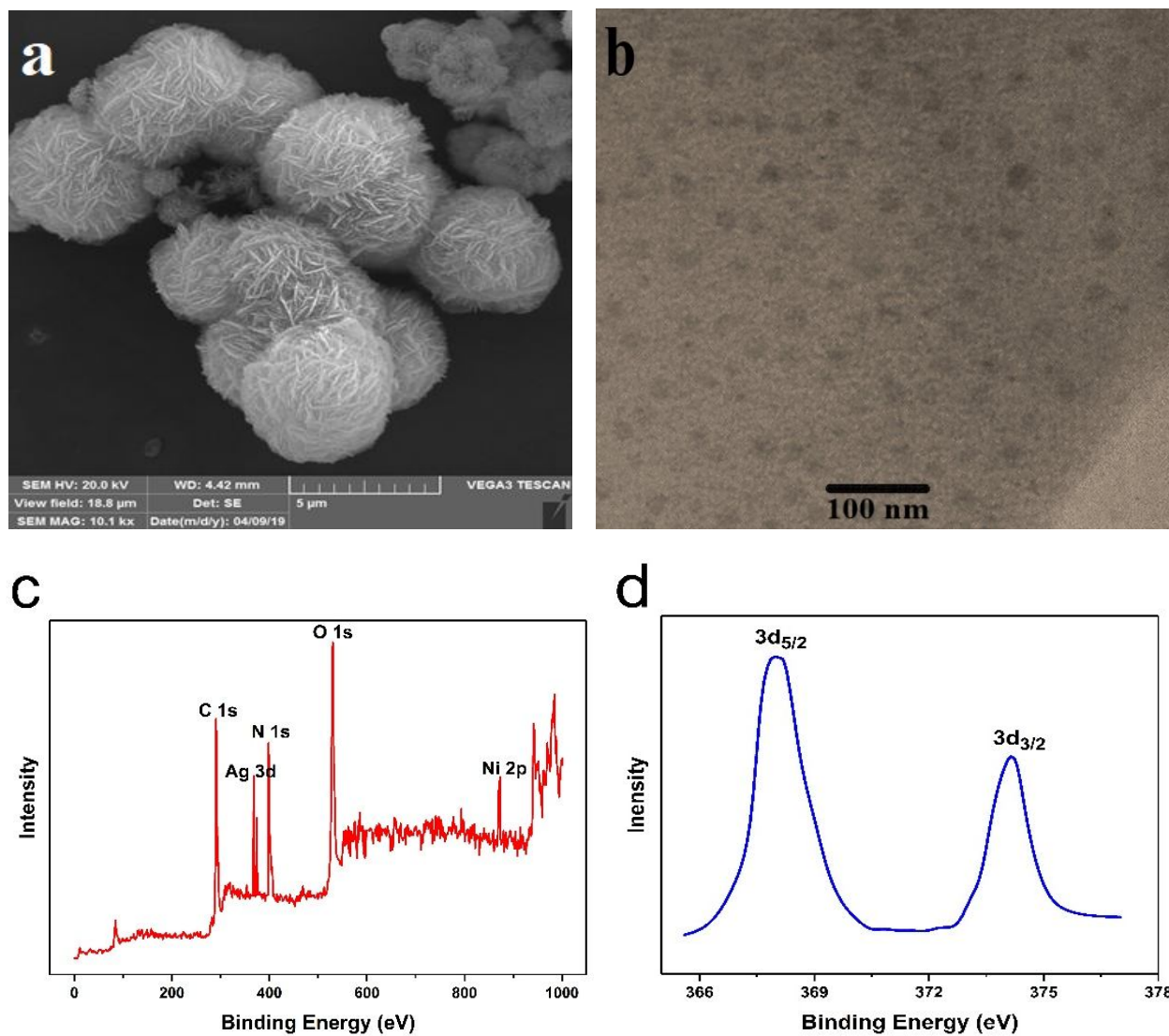
Fig. 1. XRD patterns of the prepared samples (up), TGA and DTA curve of Fe<sub>2</sub>O<sub>3</sub>@SiO<sub>2</sub>@MOF@Ag (down).



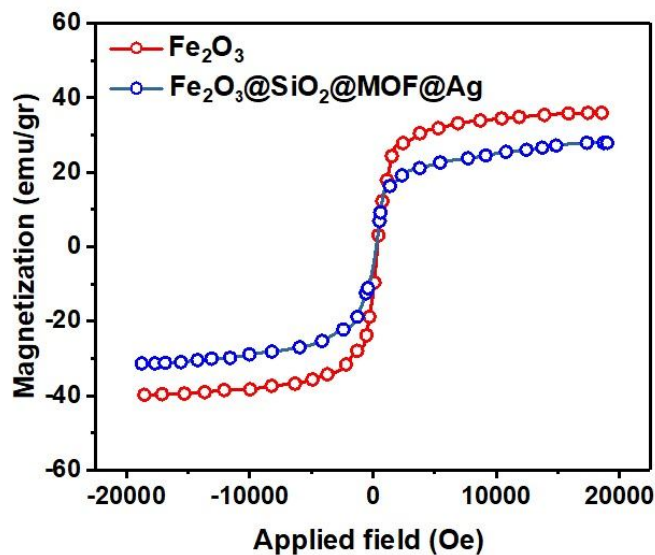
**Fig. 2.** Adsorption-desorption and BJH curve of  $\text{Fe}_2\text{O}_3$  (a,b),  $\text{Fe}_2\text{O}_3@SiO_2$  (c,d),  $\text{Fe}_2\text{O}_3@SiO_2@MOF$  and  $\text{Fe}_2\text{O}_3@SiO_2@MOF@Ag$  (e,f).

**Table 1.** BET Surface Area and Total Pore Volume of the Materials

	$S_{\text{BET}}$ ( $\text{m}^2 \text{g}^{-1}$ )	$V_a$ ( $\text{cm}^3 \text{g}^{-1}$ )	$r_{\text{p,peak}}$ ( $\text{Vol nm}^{-1}$ )
$\text{Fe}_2\text{O}_3$	2.26	1.02	53.2
$\text{Fe}_2\text{O}_3@\text{SiO}_2$	51.85	0.42	25.7
$\text{Fe}_2\text{O}_3@\text{SiO}_2@\text{MOF}$	78.1	0.16	1.87
$\text{Fe}_2\text{O}_3@\text{SiO}_2@\text{MOF}@Ag$	79.9	0.16	1.87



**Fig. 3.** SEM image of  $\text{Fe}_2\text{O}_3@\text{SiO}_2@\text{MOF}@Ag$  (a), TEM image of silver nanoparticles (b) and XPS spectra of final composite (c,d).

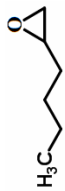
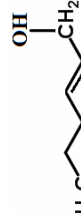
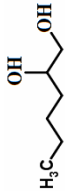


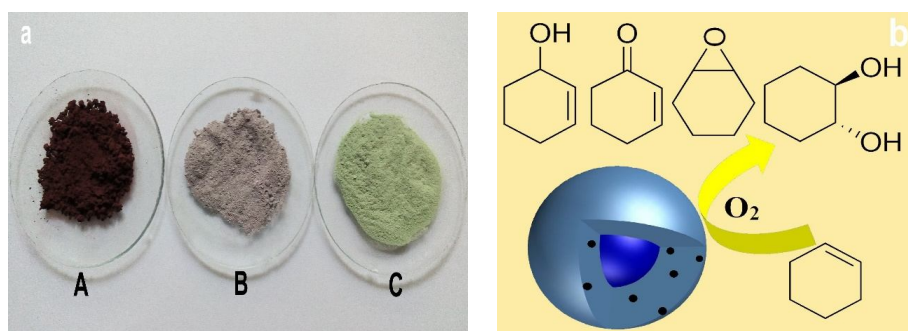
**Fig. 4.** Vibrating sample magnetometer (VSM) curve of  $\text{Fe}_2\text{O}_3$  and  $\text{Fe}_2\text{O}_3@\text{SiO}_2@\text{MOF}@\text{Ag}$  at room temperature.

**Table 2.** Selective Oxidation of Cyclohexene. Solvent = Toluene,  $T = 85\text{ }^\circ\text{C}$ , Time = 6 h, [Catal.] = 5 mg,  $P = 5$  bar

Catalyst	Conversion (%)	$\Sigma C_6$ . Sel.	TOF ( $\text{h}^{-1}$ )	Selectivity (%)			
							
$\text{Fe}_2\text{O}_3@\text{SiO}_2@\text{MOF}$	2	-	-	-	-	-	-
$\text{Fe}_2\text{O}_3@\text{SiO}_2@\text{MOF}@\text{Ag}$ (0.5%)	40.5	98	283	90.0	1.0	3.8	3.1
$\text{Fe}_2\text{O}_3@\text{SiO}_2@\text{MOF}@\text{Ag}$ (1%)	45.4	99	159	88.1	1.5	3.8	2.7
$\text{Fe}_2\text{O}_3@\text{SiO}_2@\text{MOF}@\text{Ag}$ (5%)	51.7	98	36	88.0	2	5	5
$\text{Fe}_2\text{O}_3@\text{SiO}_2@\text{MOF}@\text{Ag}$ (10%)	58.8	99	20	91.2	2	4	0.8
$\text{Fe}_2\text{O}_3@\text{SiO}_2@\text{MOF}@\text{Ag}$ (20%)	68.2	99	12	90.0	1.5	4.5	4

**Table 3.** Selective Oxidation of 1-Hexene. Solvent = Toluene, T = 85 °C, Time = 6 h, [Catal.] = 5 mg, P = 5 bar

Catalyst	Conversion (%)	$\Sigma C_6$ Sel.	TOF (h <sup>-1</sup> )	Selectivity (%)			
							
Fe <sub>2</sub> O <sub>3</sub> @SiO <sub>2</sub> @MOF	4	-	-	-	-	-	-
Fe <sub>2</sub> O <sub>3</sub> @SiO <sub>2</sub> @MOF@Ag (0.5%)	42.5	98	243	92.0	1.5	5.6	0.8
Fe <sub>2</sub> O <sub>3</sub> @SiO <sub>2</sub> @MOF@Ag (1%)	46.0	99	132	89.0	1.5	4.3	5.2
Fe <sub>2</sub> O <sub>3</sub> @SiO <sub>2</sub> @MOF@Ag (5%)	49.1	98	28	90.0	1.8	5.7	2.5
Fe <sub>2</sub> O <sub>3</sub> @SiO <sub>2</sub> @MOF@Ag (10%)	56.7	99	16	85.0	3.5	6.9	4.6
Fe <sub>2</sub> O <sub>3</sub> @SiO <sub>2</sub> @MOF@Ag (20%)	63.8	99	9	90.0	2.3	5.1	2.6



*Scheme 1.* Prepared samples (a). Fe<sub>2</sub>O<sub>3</sub> (A), Fe<sub>2</sub>O<sub>3</sub>@SiO<sub>2</sub> (B), Fe<sub>2</sub>O<sub>3</sub>@SiO<sub>2</sub>@MOF (C) and schematic catalytic reaction (b)

magnetization. This effect is related to diluting contribution of non-magnetic structure in catalysts volume.

The catalytic activity of silver nano composites with different weight percentages of silver are reported in Tables 2 and 3. In the absence of silver nanocomposites, no activity

was observed. It can be seen that the catalysts with 20 weight percent of silver have higher conversion. The selectivity is directed towards cyclohexene oxide and hexene oxide for cyclohexene and hexane reagents, respectively. The silver contents were 0.5, 1, 5, 10 and 20

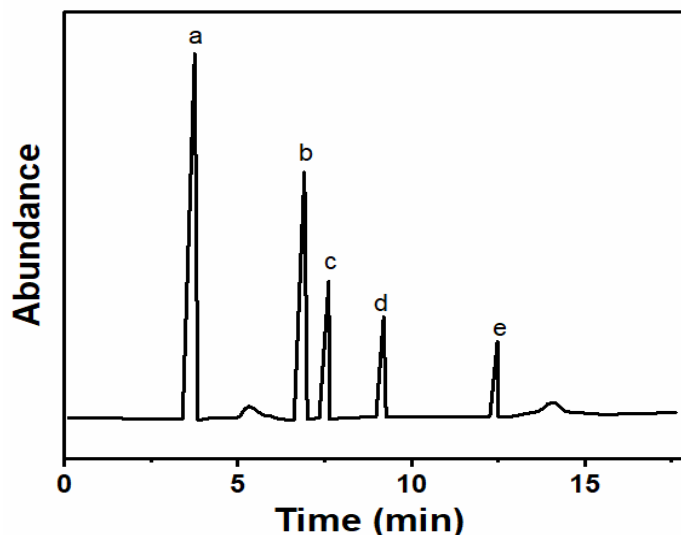


**Fig. 5.** Gas chromatogram of cyclohexene (a) and products: cyclohexene oxide (b), 2-cyclohexene-1-ol (c), 2-cyclohexene-1-one (d), and 1,2-cyclohexane diol (e).

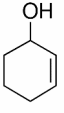
weight percent. The results indicated that silver nanoparticles have similar mean size between 20 to 25 nm. More than 98% C<sub>6</sub> selectivity observed for hexane and cyclohexane (Scheme 1). The gas chromatogram of cyclohexene and all products is demonstrated in Fig. 5. The amount of silver in catalysts is important in activity. With increasing the silver weight percentage, the conversion was increased from 40.5% to 68.2%. For cyclohexene and 1-hexane no changes were observed for product selectivity. TOF was calculated by moles of alkenes consumed per silver atom per hour which reported by h<sup>-1</sup>.

TOF of reaction decreased with the amount of silver in nanocomposites. High catalytic activity demonstrated that silver nanoparticles supported on MOF surface could active oxygen. The aerobic oxidation of alkenes and the epoxidation of alkenes at room temperature with molecular oxygen in the presence of an aldehyde and a copper salt catalyst such as copper(II) hydroxide were investigated by Murahashi and coworkers. High turnover numbers have been obtained for the oxidation of cyclohexane using a combination of copper(II) chloride and a crown ether as a catalyst [29]. A homogeneous silver(I)-catalyzed aerobic oxidation of aldehydes in water was reported by Chao-Jun Li. Different aliphatic and aromatic aldehydes were selected and all of them successfully underwent aerobic oxidation.

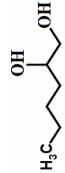
Corresponding carboxylic acids in high yields were obtained [30]. Mathew D. Hughes and coworkers investigated the solvent effect on catalytic activity of Au/C in aerobic oxidation of cyclohexene and cis-cyclooctene [31]. They demonstrated that polar solvent like water had 100% conversion but not any C<sub>6</sub> and C<sub>9</sub> products were observed. Aprotic nonpolar solvent such as Hexane, Toluene, 1,4-Dimethylbenzene, 1,3,5-Trimethylbenzene are proper options for investigation of aerobic oxidation because O<sub>2</sub> has a good solubility in these solvents and burning has not taken place. Oxidation catalytic activity in different solvents are reported in Tables 4 and 5. Our experimental tests showed that Toluene with high boiling temperature and high oxygen solubility is an excellent candidate for alkene oxidation under mild conditions. Solvent with weak interactions by nanoparticles on metal organic frameworks affect the electron transfer and could reinforce the conversion of intermediates to the preferred product. We have not used any initiator (H<sub>2</sub>O<sub>2</sub> or t-butyl hydroper-oxide) and promotor (Sn, Sb, Bi and Pb) in this work. In view of these promising results, this catalytic system with high selectivity for epoxide has great potential for oxidation of C=C.

Strongly bonded atomic oxygen which is intrinsic to silver surface causes highly selective epoxidation reaction

**Table 4.** Solvent Effects on Selective Oxidation of Cyclohexene. T = 85 °C, Time = 6 h, [Catal.] = 5 mg, P = 5 bar, Weight Percent of Silver = 0.5%

Solvent	Conversion (%)	$\Sigma C_6$ . Sel.	TOF (h <sup>-1</sup> )	Selectivity (%)			
							
Toluene	40.5	98	285	91.0	1.2	4.6	3.1
1,3,5-Trimethylbenzene	45.4	99	3198	89.9	1.2	5.6	3.0
1,4-Dimethylbenzene	51.7	98	363	89.8	1.3	5.5	3.1
Hexane	56	99	393	90.0	1.1	5.5	3.1
Water	75	-	-	-	-	-	-
Ethanol	4	-	-	-	-	-	-

**Table 5.** Solvent Effects on Selective Oxidation of 1-Hexene. T = 85 °C, Time = 6 h, [Catal.] = 5 mg, P = 5 bar, Weight Percent of Silver = 0.5%

Solvent	Conversion (%)	$\Sigma C_6$ . Sel.	TOF (h <sup>-1</sup> )	Selectivity (%)			
							
Toluene	42.5	98	244	85.0	2.0	8.0	5.0
1,3,5-Trimethylbenzene	48	99	276	89.0	1.5	6.3	3.2
1,4-Dimethylbenzene	48	98	276	90.0	1.4	3.5	5.1
Hexane	57	99	327	90.0	2.0	3.8	4.2
Water	80	-	-	-	-	-	-
Ethanol	5	-	-	-	-	-	-

[32]. Electrophilic attack by oxygen which is adsorbed atomic on surface is a major step in aerobic oxidation mechanism. Charge transfer from silver to adsorbed oxygen

could facilitate the electrophilic attack [32].

Magnetic separation and reusability are important factors for a magnetic structure. Reusability tests were

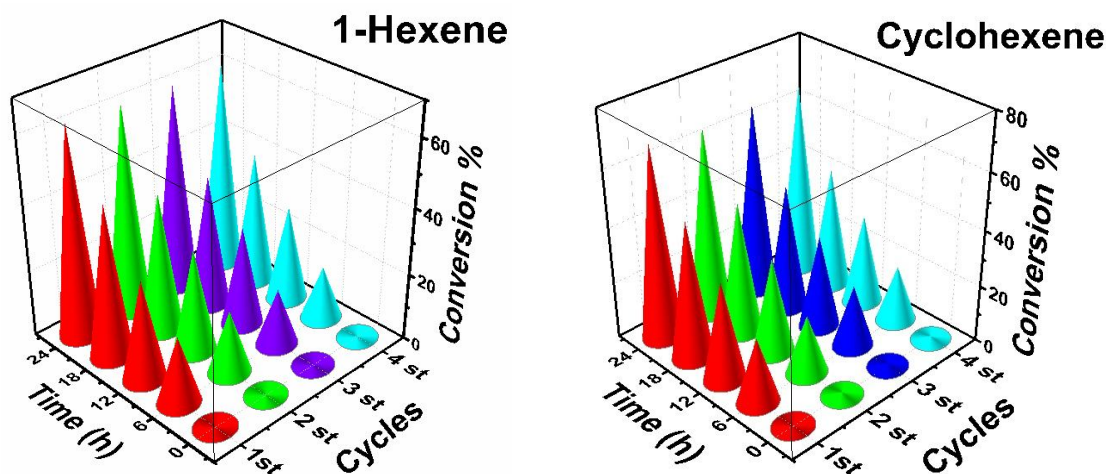


Fig. 6. Reusability tests for  $\text{Fe}_2\text{O}_3@\text{SiO}_2@\text{MOF}@\text{Ag}(20\%)$ .

performed for  $\text{Fe}_2\text{O}_3@\text{SiO}_2@\text{MOF}@\text{Ag}(20\%)$  catalysts in toluene solvent, and results indicated that after four consecutive cycles, the conversion values remain constant. As shown in Fig. 6, magnetic core shell truncated cube structure is a versatile catalyst with reasonable properties which could be a promising candidate in practical catalysis fields.

## CONCLUSIONS

Composite system of silver nanoparticles supported on  $\text{Fe}_2\text{O}_3@\text{SiO}_2@\text{Metal organic framework}$  was prepared and the results showed that this composite has potential to be an active catalysts for aerobic oxidation of alkenes under mild conditions. No initiator ( $\text{H}_2\text{O}_2$  or t-butyl hydroper-oxide) or promotor (Sn, Sb, Bi and Pb) was used in this work. According to the results, this catalytic system with high selectivity for epoxide has a great potential for oxidation of C=C.

## REFERENCES

- [1] Schlichte, K.; Kratzke, T.; Kaskel, S., Improved synthesis, thermal stability and catalytic properties of the metal-organic framework compound  $\text{Cu}_3(\text{BTC})_2$ . *Microporous and Mesoporous Materials*, **2004**, *73*, 81-88, DOI: 10.1016/j.micromeso.2003.12.027.
- [2] Gomez-Lor, B., *et al.*, Novel 2D and 3D indium metal-organic frameworks: Topology and catalytic properties. *Chem. Mater.*, **2005**, *17*, 2568-2573, DOI: 10.1021/cm047748r.
- [3] García-García, P.; Müller, M.; Corma, A., MOF catalysis in relation to their homogeneous counterparts and conventional solid catalysts. *Chem. Sci.*, **2014**, *5*, 2979-3007, DOI: 10.1039/C4SC00265B.
- [4] Wu, C.D., *et al.*, A homochiral porous metal-organic framework for highly enantioselective heterogeneous asymmetric catalysis. *J. Am. Chem. Soc.*, **2005**, *127*, 8940-1, DOI: 10.1021/ja052431t.
- [5] Xiao, L., *et al.*, Highly sensitive electrochemical sensor for chloramphenicol based on MOF derived exfoliated porous carbon. *Talanta*, **2017**, *167*, 39-43, DOI: 10.1016/j.talanta.2017.01.078.
- [6] Yan, L., *et al.*, *In situ* synthesis strategy for hierarchically porous  $\text{Ni}_2\text{P}$  polyhedrons from MOFs templates with enhanced electrochemical properties for hydrogen evolution. *ACS Appl. Mater. Interfaces*, **2017**, *9*, 11642-11650, DOI: 10.1021/acsami.7b01037.
- [7] Chen, T. -Y., *et al.*, Metal-organic framework/sulfonated polythiophene on carbon cloth as a flexible counter electrode for dye-sensitized solar cells. *Nano Energy*, **2017**, *32*, 19-27, DOI: 10.1016/j.nanoen.2016.12.019.

- [8] Xie, Z., *et al.*, Metal-organic framework derived CoNi@ CNTs embedded carbon nanocages for efficient dye-sensitized solar cells. *Electrochim. Acta*, **2017**. 229, 361-370, DOI: 10.1016/j.electacta.2017.01.145.
- [9] Li, W., *et al.*, High temperature ferromagnetism in  $\pi$ -conjugated two-dimensional metal-organic frameworks. *Chem. Sci.*, **2017**. 8, 2859-2867, DOI: 10.1039/C6SC05080H.
- [10] Rice, A. M.; Dolgoplova, E. A.; Shustova, N. B., Fulleritic materials: Buckyball-and buckybowl-based crystalline frameworks. *Chem. Mater.*, **2017**. 29, 7054-7061, DOI: 10.1021/acs.chemmater.7b02245.
- [11] Bobbitt, N. S.; Chen, J.; Snurr, R. Q., High-throughput screening of metal-organic frameworks for hydrogen storage at cryogenic temperature. *J. Phys. Chem. C*, **2016**. 120, 27328-27341. DOI: 10.1021/acs.jpcc.6b08729.
- [12] Bon, V., Metal-organic frameworks for energy-related applications. *Curr. Opin. in Green Sustainable Chem.*, **2017**. 4, 44-49. DOI: 10.1016/j.cogsc.2017.02.005.
- [13] Jiang, H. -L.; Xu, Q., Porous metal-organic frameworks as platforms for functional applications. *Chem. Commun.*, **2011**. 47, 3351-3370, DOI: 10.1039/C0CC05419D.
- [14] Dhakshinamoorthy, A.; Garcia, H., Catalysis by metal nanoparticles embedded on metal-organic frameworks. *Chem. Soc. Rev.*, **2012**. 41, 5262-5284, DOI: 10.1039/C2CS35047E.
- [15] Aijaz, A.; Xu, Q., Catalysis with metal nanoparticles immobilized within the pores of metal-organic frameworks. *J. Phys. Chem. Lett.*, **2014**. 5, 1400-1411, DOI: 10.1021/jz5004044.
- [16] Schröder, F.; Fischer, R. A., Doping of Metal-organic Frameworks with Functional Guest Molecules and Nanoparticles, in *Functional Metal-Organic Frameworks: Gas Storage, Separation and Catalysis*. 2009, Springer, 77-113, DOI: 10.1007/128-2009-4.
- [17] Zhao, Y., *et al.*, Ru nanoparticles immobilized on metal-organic framework nanorods by supercritical CO<sub>2</sub>-methanol solution: highly efficient catalyst. *Green Chem.*, **2011**. 13, 2078-2082, DOI: 10.1039/C1GC15340D.
- [18] Hermes, S., *et al.*, Metal@ MOF: Loading of highly porous coordination polymers host lattices by metal organic chemical vapor deposition. *Angewandte Chemie International Edition*, **2005**. 44, 6237-6241. DOI: 10.1002/anie.200462515.
- [19] Schröder, F., *et al.*, Simultaneous Gas-Phase Loading of MOF-5 with Two Metal Precursors: towards Bimetallics@ MOF. *European J. Inorg. Chem.*, **2009**. 2009, 3131-3140, DOI: 10.1002/ejic.200900138.
- [20] Ameloot, R., *et al.*, Metal-organic framework single crystals as photoactive matrices for the generation of metallic microstructures. *Adv. Mater.*, **2011**. 23, 1788-1791. DOI: 10.1002/adma.201100063.
- [21] Wang, C.; DeKrafft, K. E.; Lin, W., Pt nanoparticles@photoactive metal-organic frameworks: efficient hydrogen evolution via synergistic photoexcitation and electron injection. *J. Am. Chem. Soc.*, **2012**. 134, 7211-7214, DOI: 10.1021/ja300539p.
- [22] El-Shall, M. S., *et al.*, Metallic and bimetallic nanocatalysts incorporated into highly porous coordination polymer MIL-101. *J. Mater. Chem.*, **2009**. 19, 7625-7631, DOI: 10.1039/B912012B.
- [23] Jiang, H. -L., *et al.*, Au@ZIF-8: CO oxidation over gold nanoparticles deposited to metal-organic framework. *J. Am. Chem. Soc.*, **2009**. 131, 11302-11303, DOI: 10.1021/ja9047653.
- [24] Lu, G., *et al.*, Imparting functionality to a metal-organic framework material by controlled nanoparticle encapsulation. *Nat. Chem.*, **2012**. 4, 310, DOI: 10.1038/nchem.1272.
- [25] Brust, M., *et al.*, C60 mediated aggregation of gold nanoparticles. *J. Am. Chem. Soc.*, **1998**. 120, 12367-12368, DOI: 10.1021/ja982776u.
- [26] Israr, F., *et al.*, Scope of various solvents and their effects on solvothermal synthesis of Ni-BTC. *Química Nova*, **2016**. 39, 669-675, DOI: 10.5935/0100-4042.20160068.
- [27] Salari, H., Kinetics and mechanism of enhanced photocatalytic activity under visible light irradiation using Cr<sub>2</sub>O<sub>3</sub>/Fe<sub>2</sub>O<sub>3</sub> nanostructure derived from bimetallic metal organic framework. *J. Environ. Chem. Engin.*, **2019**. 7, 103092-103099, DOI: 10.1016/j.jece.2019.103092.
- [28] Salari, H.; Sadeghinia, M., MOF-templated synthesis of nano Ag<sub>2</sub>O/ZnO/CuO heterostructure for photocatalysis. *J. Photochem. Photobiol. A:*

- Chem.*, **2019**, *376*, 279-287, DOI: 10.1016/j.jphotochem.2019.03.010.
- [29] Komiya, N.; Naota, T.; Oda, Y.; Murahashi, S. I., Aerobic oxidation of alkanes and alkenes in the presence of aldehydes catalyzed by copper salts and copper-crown ether. *J. Mol. Catal. A: Chem.*, **1997**, *117*, 21-37, DOI: 10.1016/S1381-1169(96)00263-4.
- [30] Liu, M.; Wang, H.; Zeng, H.; Li, C. J., Silver(I) as a widely applicable, homogeneous catalyst for aerobic oxidation of aldehydes toward carboxylic acids in water "silver mirror": From stoichiometric to catalytic. *Sci. Adv.*, **2015**, *1*, e1500020, DOI: 10.1126/sciadv.1500020.
- [31] Hughes, M. D., *et al.*, Tunable gold catalysts for selective hydrocarbon oxidation under mild conditions. *Nature*, **2005**, *437*, 1132-5, DOI: 10.1038/nature04190.
- [32] Hawker, S., *et al.*, Molecular mechanism of heterogeneous alkene epoxidation: A model study with styrene on Ag (111). *Surface Sci.*, **1989**, *219*, L615-L622. DOI: 10.1016/0039-6028(89)90509-8.